

Dynamic modeling and vibration analysis of a flexible gear transmission system

Jing Liu^{1),2)}*, Xinbin Li^{1),2)}, Ruikun Pang³⁾, Min Xia⁴⁾

1) School of Marine Science and Technology, Northwestern Polytechnical University, Xi'an, 710072, People's Republic of China

2) Laboratory for Unmanned Underwater Vehicle, Northwestern Polytechnical University, Xi'an, 710072, People's Republic of China

3) College of Mechanical Engineering, Chongqing University, Chongqing, 400030, People's Republic of China

4) Department of Engineering, Lancaster University, Lancaster, LA1 4YW, United Kingdom

*Corresponding author: Jing Liu. Email: jliu@cqu.edu.cn; jliu0922@nwpu.edu.cn.

Abstract

Vibrations of gear transmission systems (GTSs) are the key problems in the machinery industry. In the previous vibration analysis of GTS, the rotor is usually regarded as a rigid part. The rigid-shaft gear-transmission dynamic system (RGDS) model cannot solve the differences of vibrations of rotor at different axial positions. To solve this problem, a flexible-shaft gear-transmission system dynamic (FGDS) model is established by using the finite element method. In the FGDS, the GTSs is separated into some flexible shaft segments, gear meshing unit and bearing unit. The bearing stiffness, bearing contact force, time-varying meshing stiffness and damping force of gear are considered. The time- and frequency-domain vibrations of FGDS and RGDS model under different rotational speeds are compared and analyzed. Note that the FGDS can obtain more accurate results than the RGDS model. The vibrations from FGDS are less than those from RGDS model. This paper can give some new approach for the dynamic modeling and vibration analysis of flexible GTSs.

Keywords: Flexible shaft; vibrations; bearing; gear; dynamic modelling

1. Introduction

As an important part, gear-transmission-systems (GTSs) are used in the various transmission machinery [1,2,3]. **The GTSs consist of shafts, rolling bearing, and gears. The vibrations of the GTSs are complex and difficult to be analyzed and diagnosed. A more comprehensive dynamic model of GTSs can be helpful for the vibrations analysis and fault diagnosis.**

Many works were focused on the vibrations of the rotor system. Neriya et al. [4] used a FE method to simulate the bending-torsional coupling vibrations of gear transmission system. Zhu et al. [5] proposed a GTS dynamic model considering the elastic support of gearbox. Liu et al. [6] established a gear transmission dynamic model to study the nonlinear characteristics of a gear pair with variable center distance. Howard et al. [7] established a simplified gear transmission system dynamic model, which considered the gear tooth torsion and time-varying meshing stiffness. Mohamme et al. [8] established a gear transmission model and studied the vibrations along the meshing line. Bozca et al. [9] established a gear transmission system model and found that the vibrations of gear box could be reduced by reducing the transmission error of gear pair. Theodossiades et al. [10] proposed a gear transmission model to estimate the vibrations of gear pairs under different working conditions. Dikmen et al. [11] proposed a finite-element (FE) model for analyzing the influence of the bearing stiffness on the natural frequencies of flexible shaft system. Xi et al. [12,13] established a shaft-bearing system dynamic model based on the FE analysis and studied the relationship between the system manufacturing error and vibrations. Hamzehlouia and Behdinan [14] established a flexible multi-rotor model based on the FE theory. They studied the influence of the damping lubrication on the vibrations of rotor system. The above works

regarded the rolling bearing as spring in the study of the rotor system vibrations. Obviously, this assumption ignores the nonlinearity of the rolling bearing. The vibrations obtained by the methods in their works are unreasonable and cannot fully represent the vibrations of the rotor systems.

Moreover, some scholars studied the vibrations of the rotor system considering the rolling bearing nonlinearity [15-19]. Cao et al. [20] proposed a dynamic model of rigid shaft-bearing system considering the manufacturing error and bearing support stiffness. Liu et al. [21,22] thought the shaft and bearing house deformations have significant effects on the rotor system vibrations. They proposed an optimization method of the shaft and bearing house stiffness for a rotor system to reduce the vibrations. Li et al. [23] proposed a dynamic model for a rotor-bearing system with bolted-disk joint. They studied the effect of bolted joint stiffness on the rotor dynamic response. Jin et al. [24] proposed a dynamic model for a dual rotor system considering the nonlinearities of the supporting bearing. Liu et al. [25] introduced a flexible-rotor system dynamic model considering the effects of the nonlinear bearing contact forces. They compared the results obtained by Hertzian and cubic polynomial nonlinear contact force methods and found that cubic polynomial nonlinear contact force has a significant difference in high speed compared to Hertzian method. Cao et al. [26] studied the vibrations of a rotor-bearing-pedestal systems considering the outer ring-pedestal fit clearance. Wang and Zhu [27] established a dynamic model for a rotor system. They studied the effect of bearing on the rotor vibrations and load sharing performance.

Many works were also focused on the gear dynamic modeling. Kong et al. [28] proposed a new meshing stiffness calculation method considering the gear flexibility. They studied the gear flexibility on the vibrations of GTS. Hu et al. [29] investigated the effect of stagger angle excitations on the GTS vibrations and load sharing features. They also obtained the natural characteristics of GTS. Huangfu et al. [30] proposed a GTS dynamic model considering the flexibility of gear foundations. They used Mindlin-Reissner shell elements to model gear foundations. Wan et al. [31] proposed an improved meshing stiffness calculation method for helical gears. They studied the effects of different helical gear parameters on the mesh stiffness based on the proposed method. Through above discussions, we can find that few works investigated the effects of flexible shaft, time-varying mesh stiffness and bearing nonlinearity together. Moreover, few people focused on the multi-stage transmission system dynamic modeling. This paper will overcome this problem.

In this paper, the vibrations of a shaft-gear-bearing system is studied. Based on the FE method, a GTS considering the flexible shaft (FGDS) is established. Compared with the rigid GTS model with the same parameters, the differences of vibrations at each node under different input speeds are analyzed. The Newmark-beta method is used to simulate the dynamics of two models in the Matlab software. The simulation results in time- and frequency-domain are compared. The results show that the simulation results will be more accurate when the flexibility of shaft in the GTS is considered. This research can provide a new method and idea for dynamic modeling and vibration analysis of GTSs.

2. Dynamic modelling of FGDS

2.1 Dynamic modelling of flexible shaft segments

In this paper, the shafts of FGDS model are divided into several flexible shaft segments, which is used to realize the flexibility of shaft. [The flexible shaft needs to consider the shaft deformations in the lateral, longitudinal and torsional directions. The Timoshenko beam theory and the Euler-Bernoulli beam theory can all satisfy this requirement. The Euler-Bernoulli beam theory assume that the beam cross section is](#)

perpendicular to the central axis both before and after lateral deformation. This assumption is applicable for the slender shafts. However, the shafts in mechanical transmission systems usually cannot satisfy this assumption. Thus, the Timoshenko beam element is used to establish the dynamic model of shaft segment element based on the method in Ref. [32]. The center of cross sections at two ends of each axial segment is the node with six degrees of freedom, which can be represented by the displacement vector \mathbf{v}_g , as shown in Figure 1. The length of shaft segment is represented by l .

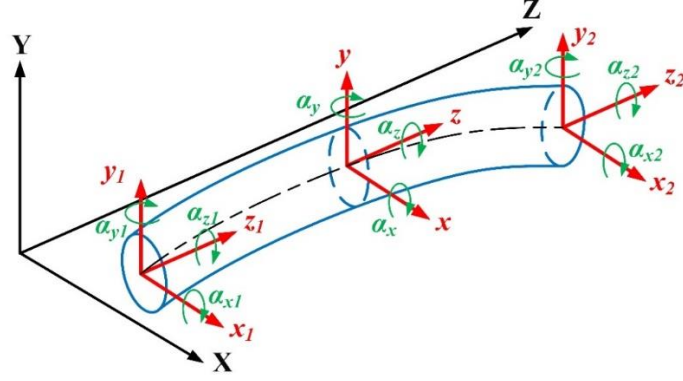


Fig 1. One element of flexible shaft segment.

The displacement vector \mathbf{v}_g is given as

$$\mathbf{v}_g = [x_1 \ y_1 \ z_1 \ \alpha_{x1} \ \alpha_{y1} \ \alpha_{z1} \ x_2 \ y_2 \ z_2 \ \alpha_{x2} \ \alpha_{y2} \ \alpha_{z2}]^T \quad (1)$$

where I_x represents the inertia moment of section of flexible shaft segment in the Y - Z coordinate plane, I_y is the inertia moment of section of flexible shaft segment in the X - Z coordinate plane. The matrix of mass inertia matrix \mathbf{M}_s can be given as

$$\mathbf{M}_s = \begin{bmatrix} \mathbf{M}_{s11} & \mathbf{M}_{s12} \\ \mathbf{M}_{s21} & \mathbf{M}_{s22} \end{bmatrix} \quad (2)$$

$$\mathbf{M}_{s11} = \frac{\rho Al}{6} \begin{bmatrix} 2 & 0 & 0 & 0 & 0 & 0 \\ 0 & 2 & 0 & 0 & 0 & 0 \\ 0 & 0 & 2 & 0 & 0 & 0 \\ 0 & 0 & 0 & 0 & 0 & 0 \\ 0 & 0 & 0 & 0 & 0 & 0 \\ 0 & 0 & 0 & 0 & 0 & \frac{2J_p}{A} \end{bmatrix} \quad \mathbf{M}_{s12} = \frac{\rho Al}{6} \begin{bmatrix} 1 & 0 & 0 & 0 & 0 & 0 \\ 0 & 1 & 0 & 0 & 0 & 0 \\ 0 & 0 & 1 & 0 & 0 & 0 \\ 0 & 0 & 0 & 0 & 0 & 0 \\ 0 & 0 & 0 & 0 & 0 & 0 \\ 0 & 0 & 0 & 0 & 0 & \frac{J_p}{A} \end{bmatrix} \quad (3)$$

$$\mathbf{M}_{s22} = \mathbf{M}_{s11} \quad \mathbf{M}_{s21} = \mathbf{M}_{s12} \quad (4)$$

where J_p is the polar inertia moment of shaft segment.

The stiffness matrix of element can be given as[25]

$$\mathbf{K}_s = \begin{bmatrix} \mathbf{K}_{s11} & \mathbf{K}_{s12} \\ \mathbf{K}_{s21} & \mathbf{K}_{s22} \end{bmatrix} \quad (5)$$

where \mathbf{K}_{s11} , \mathbf{K}_{s12} , \mathbf{K}_{s21} , and \mathbf{K}_{s22} in Eq. (5) can be expressed as

$$\mathbf{K}_{s11} = \begin{bmatrix} \frac{GA}{kl} & 0 & 0 & 0 & -\frac{GA}{2k} & 0 \\ 0 & \frac{GA}{kl} & 0 & \frac{GA}{2k} & 0 & 0 \\ 0 & 0 & \frac{EA}{l} & 0 & 0 & 0 \\ 0 & \frac{GA}{2k} & 0 & \frac{GA}{4k} + \frac{EI_x}{l} & 0 & 0 \\ -\frac{GA}{2k} & 0 & 0 & 0 & \frac{GA}{4k} + \frac{EI_y}{l} & 0 \\ 0 & 0 & 0 & 0 & 0 & \frac{GJ_p}{l} \end{bmatrix} \quad (6)$$

$$\mathbf{K}_{s12} = \begin{bmatrix} -\frac{GA}{kl} & 0 & 0 & 0 & -\frac{GA}{2k} & 0 \\ 0 & -\frac{GA}{kl} & 0 & \frac{GA}{2k} & 0 & 0 \\ 0 & 0 & -\frac{EA}{l} & 0 & 0 & 0 \\ 0 & -\frac{GA}{2k} & 0 & \frac{GA}{4k} - \frac{EI_x}{l} & 0 & 0 \\ \frac{GA}{2k} & 0 & 0 & 0 & \frac{GA}{4k} - \frac{EI_y}{l} & 0 \\ 0 & 0 & 0 & 0 & 0 & -\frac{GJ_p}{l} \end{bmatrix} \quad (7)$$

$$\mathbf{K}_{s21} = \begin{bmatrix} -\frac{GA}{kl} & 0 & 0 & 0 & -\frac{GA}{2k} & 0 \\ 0 & -\frac{GA}{kl} & 0 & -\frac{GA}{2k} & 0 & 0 \\ 0 & 0 & -\frac{EA}{l} & 0 & 0 & 0 \\ 0 & \frac{GA}{2k} & 0 & \frac{GA}{4k} - \frac{EI_x}{l} & 0 & 0 \\ -\frac{GA}{2k} & 0 & 0 & 0 & \frac{GA}{4k} - \frac{EI_y}{l} & 0 \\ 0 & 0 & 0 & 0 & 0 & -\frac{GJ_p}{l} \end{bmatrix} \quad (8)$$

$$\mathbf{K}_{s22} = \begin{bmatrix} \frac{GA}{kl} & 0 & 0 & 0 & \frac{GA}{2k} & 0 \\ 0 & \frac{GA}{kl} & 0 & -\frac{GA}{2k} & 0 & 0 \\ 0 & 0 & \frac{EA}{l} & 0 & 0 & 0 \\ 0 & -\frac{GA}{2k} & 0 & \frac{GA}{4k} + \frac{EI_x}{l} & 0 & 0 \\ \frac{GA}{2k} & 0 & 0 & 0 & \frac{GA}{4k} + \frac{EI_y}{l} & 0 \\ 0 & 0 & 0 & 0 & 0 & \frac{GJ_p}{l} \end{bmatrix} \quad (9)$$

The damping matrix of flexible axial element is calculated by combining Rayleigh damping with \mathbf{M}_s and \mathbf{K}_s [33], which is given as

$$\mathbf{C}_s = a_1 \mathbf{M}_s + a_2 \mathbf{K}_s \quad (10)$$

where a_1 and a_2 are the mass proportionality coefficients and stiffness proportionality coefficients.

The flexible shaft element is given as

$$\mathbf{M}_1 \ddot{\mathbf{v}}_g + \mathbf{C}_1 \dot{\mathbf{v}}_g + \mathbf{K}_1 \mathbf{v}_g = 0 \quad (11)$$

where $\ddot{\mathbf{v}}_g$ and $\dot{\mathbf{v}}_g$ are the acceleration and velocity vectors of flexible shaft segment derived from the second and first derivatives of \mathbf{v}_g , respectively.

2.2 Dynamic modelling of gear and bearing

The deformations of gear and bearing components during operation are mainly contact elastics deformation. The flexible deformations are not significant. The lumped parameter method can characterize their vibrations very well and save a huge amount of calculation costs. Thus, the lumped parameter method is used to establish gear and bearing dynamic models.

The helical gears are used in FGDS model. The meshing stiffness excitation and displacement excitation are mainly considered in the dynamic modeling of gear meshing unit. The two kinds of excitation exist simultaneously and interact with each other. The dynamic equation of gear meshing unit is expressed as

$$\mathbf{M}_m \ddot{\mathbf{q}}_m + \mathbf{C}_m \dot{\mathbf{q}}_m + \mathbf{K}_m (\mathbf{q}_m - \mathbf{e}) = F_s \quad (12)$$

where \mathbf{q}_m is the displacement of gear meshing element node in FGDS model. \mathbf{M}_m , \mathbf{C}_m , and \mathbf{K}_m represent the mass matrix, damping matrix and stiffness matrix of meshing element respectively. F_s represents GTS's gear meshing force; \mathbf{e} is the equivalent displacement column vector representing the meshing comprehensive error in the direction of six degrees of freedom. The matrix form of \mathbf{M}_m is given as

$$\mathbf{M}_{mp} = (\rho A_p b_p) \begin{bmatrix} m_p & 0 & 0 & 0 & 0 & 0 \\ 0 & m_p & 0 & 0 & 0 & 0 \\ 0 & 0 & m_p & 0 & 0 & 0 \\ 0 & 0 & 0 & I_{xp} & 0 & 0 \\ 0 & 0 & 0 & 0 & I_{yp} & 0 \\ 0 & 0 & 0 & 0 & 0 & I_{zp} \end{bmatrix} \quad \mathbf{M}_{mg} = (\rho A_g b_g) \begin{bmatrix} m_g & 0 & 0 & 0 & 0 & 0 \\ 0 & m_g & 0 & 0 & 0 & 0 \\ 0 & 0 & m_g & 0 & 0 & 0 \\ 0 & 0 & 0 & I_{xg} & 0 & 0 \\ 0 & 0 & 0 & 0 & I_{yg} & 0 \\ 0 & 0 & 0 & 0 & 0 & I_{zg} \end{bmatrix} \quad (13)$$

where the subscript p and g represent the driving and driven gears in FGDS model, respectively. A is the gear end area, b is the gear width, $I_x=I_y=1/12(4r_f^2+3r_i^2+b^2)$, $I_z=1/2(r_f^2+r_i^2)$, r_f represents the radius of indexing circle of gears, r_i represents the radius of hub of gears.

The stiffness matrix and damping matrix of gear meshing unit are given as

$$\mathbf{K}_m = k_m \mathbf{V}^T \mathbf{V} = \begin{bmatrix} \mathbf{K}_{m11} & \mathbf{K}_{m12} \\ \mathbf{K}_{m21} & \mathbf{K}_{m22} \end{bmatrix} \quad (14)$$

$$\mathbf{C}_m = c_m \mathbf{V}^T \mathbf{V} = \begin{bmatrix} \mathbf{C}_{m11} & \mathbf{C}_{m12} \\ \mathbf{C}_{m21} & \mathbf{C}_{m22} \end{bmatrix} \quad (15)$$

where k_m and c_m are the time-varying meshing stiffness and meshing damping of gears respectively. **The time-varying meshing stiffness calculation method is based on Ref. [34].** \mathbf{V} represents the projection vector of transformation from the displacements in all directions at the gear node to the meshing line direction, which can be expressed by [35]

$$\mathbf{V} = [\cos \beta_b \sin \phi, \pm \cos \beta_b \cos \phi, \sin \beta_b, \mp r_p \sin \beta_b \sin \phi, \\ -r_p \sin \beta_b \cos \phi, \pm r_p \cos \beta_b, -\cos \beta_b \sin \phi, \mp \cos \beta_b \cos \phi, \\ -\sin \beta_b, \mp r_g \sin \beta_b \sin \phi, -r_g \sin \beta_b \cos \phi, \pm r_g \cos \beta_b]$$
(16)

where r_p and r_g are the radius of base circle of driving and driven gears respectively. β_b represents the spiral angle of base circle. If the value is positive, it means dextral rotation; if the value is negative, it means left-handed rotation; ϕ represents the included angle between the meshing line of driving gear face and the vertical positive direction.

In the FGDS model, each shaft is equipped with two supporting bearings. During the operation of system, the outer raceway of roller bearing is fixed on the bearing bracket; the inner ring is fixed with the shaft; and the vibration will be generated by the vibration of shaft.

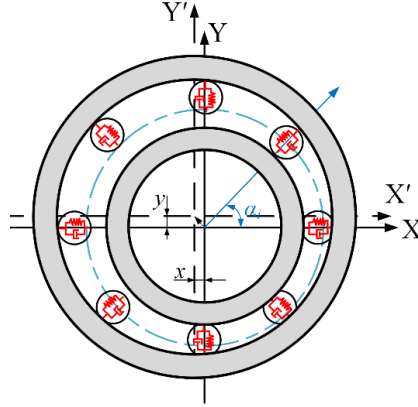


Fig 2. Dynamic model of a roller bearing.

To consider the influence of the bearing contact force on the vibrations in the FGDS model, the dynamic equation of roller bearing is calculated.

Here, there are j rollers in the roller bearing. When the i th roller is at any angle of bearing, the total contact deformation of bearing inner raceway is given as

$$\zeta_i = y \sin \alpha_i + x \cos \alpha_i - \zeta_0$$
(17)

where $i = 1, 2, \dots, j$. α_i is the angle between the i th roller and positive direction of X -axis as shown in Figure 2, which is given as

$$\alpha_i = \frac{\omega t r_i}{r_o + r_i} + \frac{2\pi(i-1)}{N_b}$$
(18)

where r_i and r_o represent the radii of inner and outer raceways. ω is the rotate speed of inner raceway. t is the time. N_b is the total rollers number.

According to the classical Hertz contact force calculation method, the contact force F_b between the rollers and raceways can be expressed as

$$F_b = K_g \zeta_i^n$$
(19)

where K_g is the Hertz contact stiffness between the raceway and i th roller [36]; n represents the load deformation coefficient, which is 3/2 for ball bearing [37,38].

The contact forces between the ring and rollers along the horizontal (X) and vertical (Y) directions are established respectively, and their expressions are as follows

$$F_X = \sum_{i=1}^{N_b} F_b(\zeta_i) J(\zeta_i) \sin \alpha_i$$
(20)

$$F_Y = \sum_{i=1}^{N_b} F_b(\zeta_i) J(\zeta_i) \cos \alpha_i$$
(21)

In Eqs. (20) and (21), $F_b(\zeta_i)$ is the contact force of i th roller of bearing when the contact

deformation is ζ_i . $J(\zeta_i)$ is a conditional function to determine whether the bearing rollers and ring have contact deformation, and its expression is given as

$$J(\zeta_i) = \begin{cases} 0 & \zeta_i \leq 0 \\ 1 & \zeta_i > 0 \end{cases} \quad (22)$$

The dynamic equation of roller bearing is given as

$$\begin{cases} m\ddot{x} + c\dot{x} + F_x = 0 \\ m\ddot{y} + c\dot{y} + F_y = 0 \end{cases} \quad (23)$$

where \dot{x} and \ddot{x} represent the speed and acceleration of inner raceway in the X direction. \dot{y} and \ddot{y} represent the speed and acceleration of inner raceway in the Y direction. m represents the mass of inner ring; and c is the contact damping between the raceways and rollers.

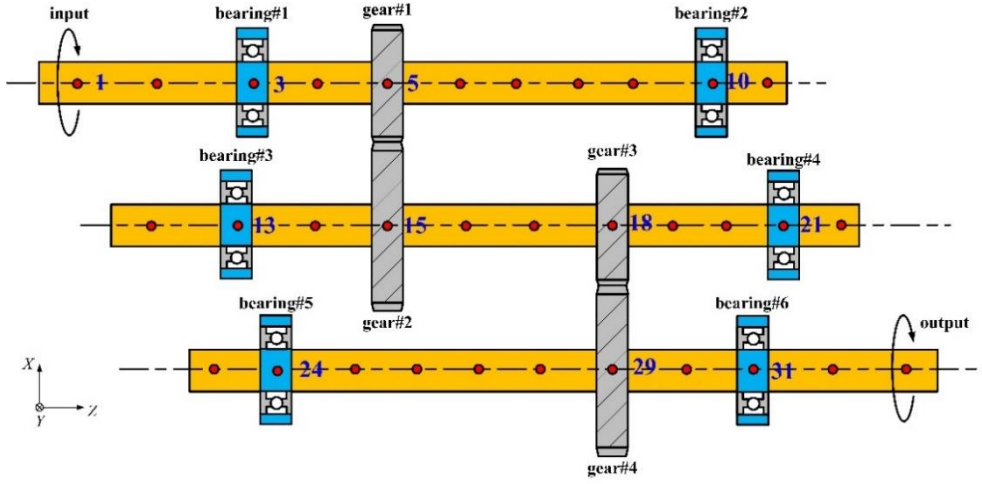


Fig 3. The proposed FGDS model.

2.3 Dynamic modelling of flexible shaft GTS

After the dynamics model of each unit is determined, the dynamics model of FGDS can be established, as is show in Figure 3. By using the dynamic equations of flexible shaft segment, gear meshing and rolling bearing, the dynamic equation of FGDS model is established as

$$\mathbf{M}\ddot{\mathbf{v}}(t) + \mathbf{C}\dot{\mathbf{v}}(t) + \mathbf{K}\mathbf{v}(t) = \mathbf{P}_0 \quad (24)$$

In the establishment of FGDS model, each shaft is divided into multiple nodes; and the center points of gears and bearings are located on the nodes. One flexible shaft segment is connected by two nodes. In Eq. (24), \mathbf{P}_0 is the forces and torques applied to the system, which includes the input and output torques, gear meshing forces, and bearing contact forces. \mathbf{M} , \mathbf{C} , and \mathbf{K} can be respectively expressed as

$$\mathbf{M} = \begin{bmatrix} \mathbf{M}_1 & 0 & 0 \\ 0 & \mathbf{M}_2 & 0 \\ 0 & 0 & \mathbf{M}_3 \end{bmatrix} \quad (25)$$

$$\mathbf{K} = \begin{bmatrix} \mathbf{K}_1 + \mathbf{K}_{m11} & \mathbf{K}_{m12} & 0 \\ \mathbf{K}_{m21} & \mathbf{K}_2 + \mathbf{K}_{m22} + \mathbf{K}_{m33} & \mathbf{K}_{m34} \\ 0 & \mathbf{K}_{m43} & \mathbf{K}_3 + \mathbf{K}_{m44} \end{bmatrix} \quad (26)$$

$$\mathbf{C} = \begin{bmatrix} \mathbf{C}_1 + \mathbf{C}_{m11} & \mathbf{C}_{m12} & 0 \\ \mathbf{C}_{m21} & \mathbf{C}_2 + \mathbf{C}_{m22} + \mathbf{C}_{m33} & \mathbf{C}_{m34} \\ 0 & \mathbf{C}_{m43} & \mathbf{C}_3 + \mathbf{C}_{m44} \end{bmatrix} \quad (27)$$

Young's modulus /E	209 Gpa	209 Gpa
Poisson's ratio / ν	0.30	0.30
Tooth width	40 mm	40mm
Module	1.5mm	1.5 mm
Teeth number	22	81
Pressure angle	20°	20°
Spiral angle	15°	15°
Addendum coefficient	1	1
Tip clearance coefficient	0.25	0.25

Table 2. Supporting bearing parameters

Parameters	Value
Inner diameter D_{in} (mm)	20
Outer diameter D_{ou} (mm)	52
Width B_h (mm)	23
Pitch diameter D (mm)	36
Ball diameter d (mm)	10.53
Ball number Z	6
Outer ring groove curvature radius r_{ou} (mm)	5.58
inner ring groove curvature radius r_{in} (mm)	5.47
Clearance C_r (μm)	10
Contact angle α (°)	0

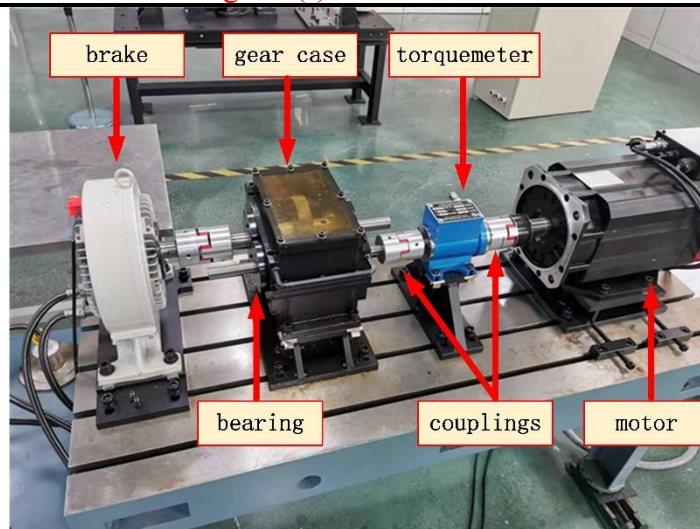


Fig. 4. A shaft gear bearing system test bench.

The time-domain experimental results and simulation results of vibration acceleration of bearing 1 in the X - and Y -directions at the input rotate speed of 2500 r/min are shown in Figure 5. Experimental test spectrum and simulation spectrum of vibration acceleration of bearing in Y -direction are shown in Figure 5 respectively. It can be seen from the figures that in the experimental spectrum and the calculated spectrum within 3000Hz, the characteristic frequencies are mainly f_i and $3f_i$, $5f_i$, $6f_i$, $8f_i$ and $9f_i$ of the rolling body of the bearing passing through the raceway. The characteristic frequency errors of measured acceleration spectrum and simulated acceleration spectrum are less than 1%. **The simulation results and experimental results are in good agreement, and this indicates the correctness of the proposed model to a certain extent.**

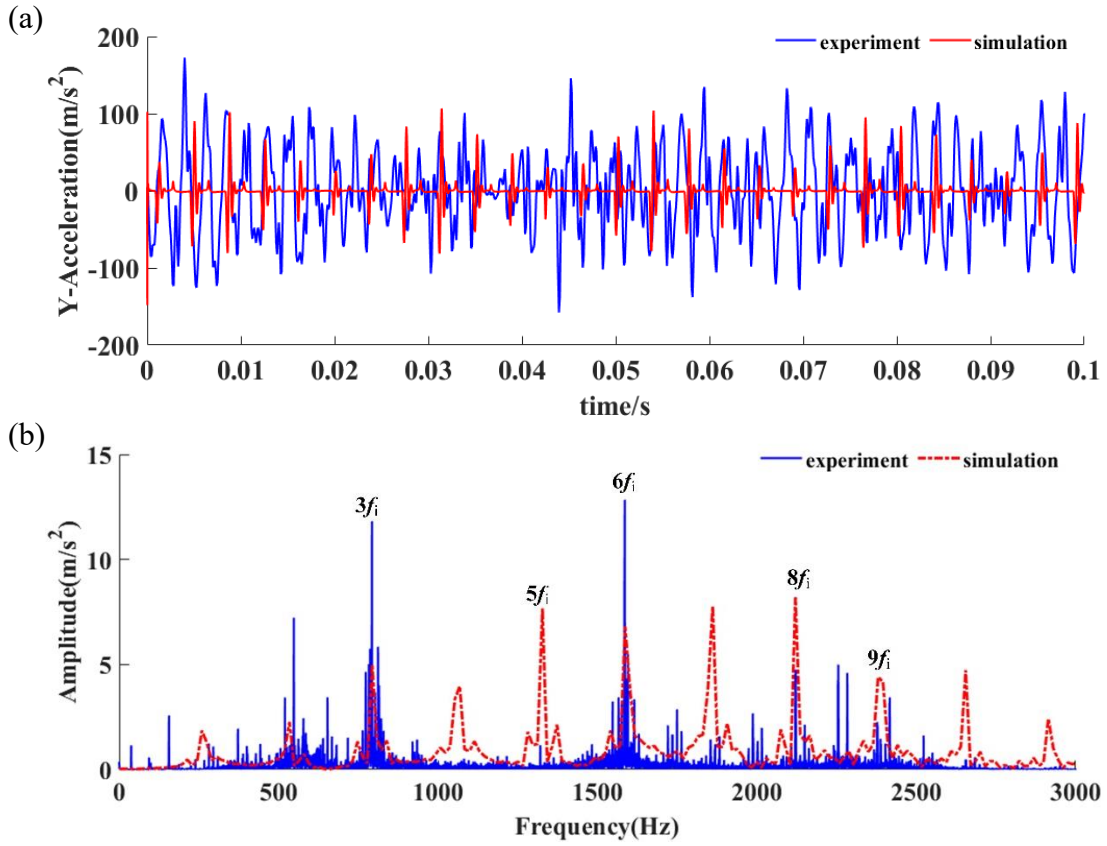


Fig. 5. Comparisons of the Y-direction accelerations from the experiment and simulation at the bearing 1 for the input rotate speed of 2500r/min.

3. Results and discussions

To analyze the influence of the shaft flexibility on the vibrations of GTSSs, a RGDS model is established without considering the flexible shaft, the shafts are regarded as the rigid bodies in RGDS model. The element modeling method of RGDS model is the same as that of FGDS model. The Newmark-beta integral method is used to solve the dynamic equations of RGDS model and FGDS model. By using the Fast Fourier Transformation (FFT) method, the spectra of accelerations along the Y- and Z-direction of bearings of RGDS model and FGDS model are obtained and compared. This work shows the vibrations of bearings to avoid too many similar results in the text. The gear parameters used in FGDS model are shown in Table 3.

Table 3. Gear parameters in FGDS model and RGDS model.

Parameters	gear#1	gear#2	gear#3	gear#4
Material	40Cr	40Cr	40Cr	40Cr
Young's modulus/ E	209 Gpa	209 Gpa	209 Gpa	209 Gpa
Poisson's ratio/ ν	0.30	0.30	0.30	0.30
Width/ B	40mm	40mm	40mm	40mm
Modulus	4.5mm	4.5mm	4mm	4mm
Number of teeth	39	117	44	132
Pressure angle	20°	20°	20°	20°
Spiral Angle	13.5°	13.5°	13.5°	13.5°
Rotation direction	right	left	right	left
Height coefficient				

3.1 Vibrations analysis of FGDS in Y direction

In this section, the vibrations of FGDS in Y direction from the proposed and RGDS models are compared. The results for the input shaft rotate speed from 2000r/min to 4000r/min are analyzed. The input torque is 500Nm in the following analysis.

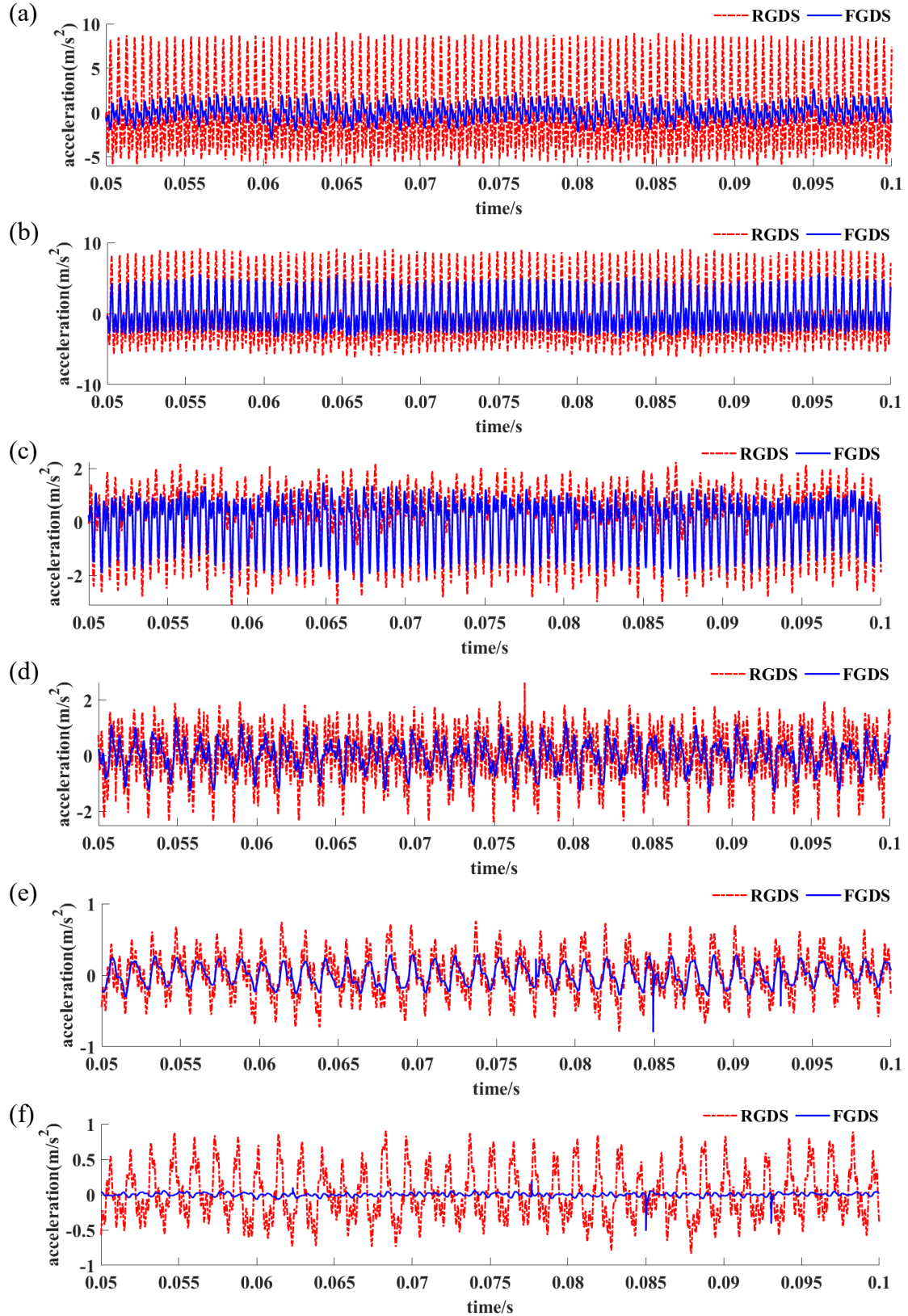


Fig 6. Comparisons of time-domain accelerations of support bearings from FGDS model and RGDS model in the Y direction. (a) Bearing#1, (b) bearing#2, (c) bearing#3, (d) bearing#4, (e) bearing#5, and (f) bearing#6.

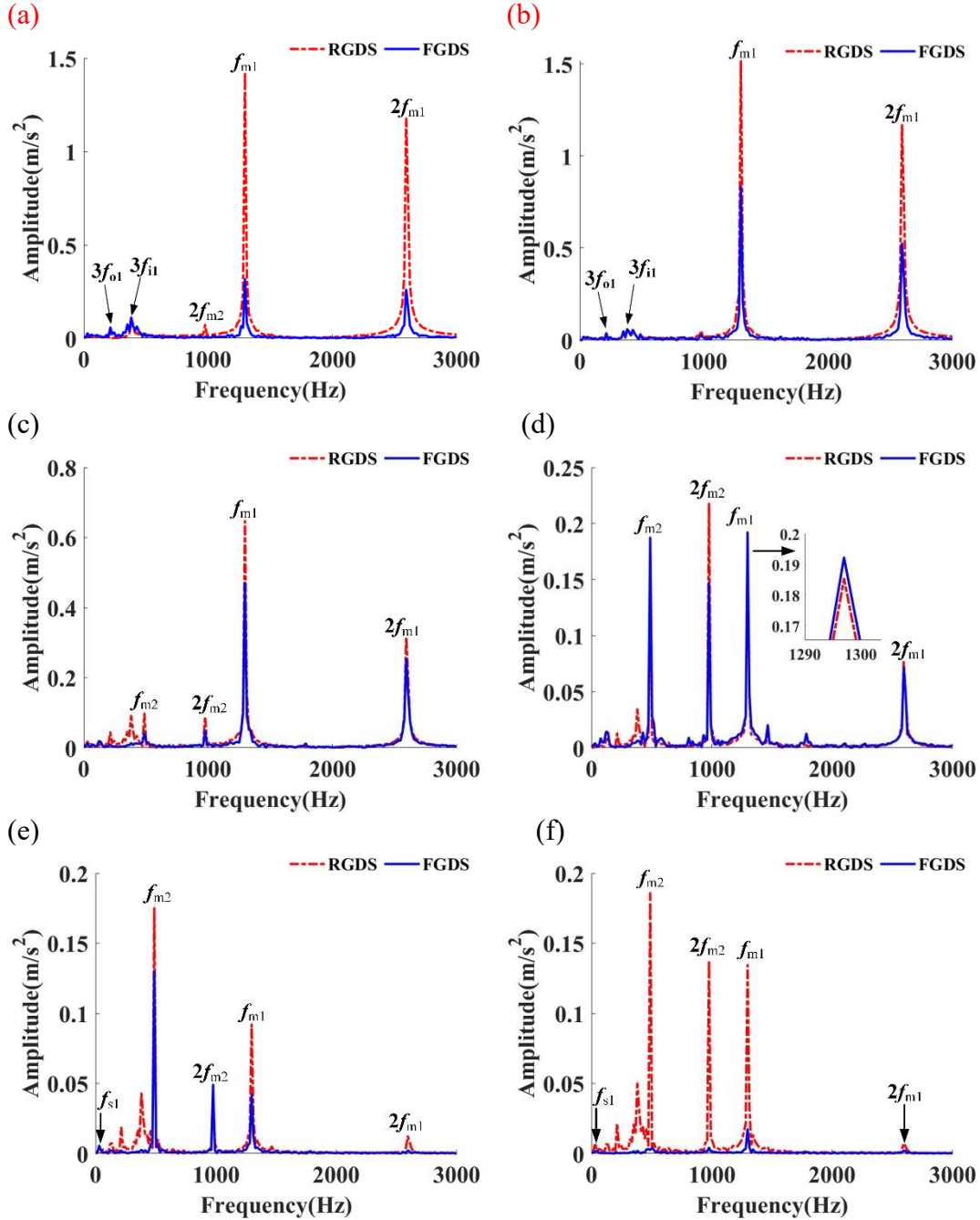


Fig 7. Comparisons of frequency-domain accelerations of support bearings from the FGDS model and RGDS model in the Y direction when the input shaft rotate speed is 2000r/min. (a) Bearing#1, (b) bearing#2, (c) bearing#3, (d) bearing#4, (e) bearing#5, and (f) bearing#6.

To analyze the difference of spectra between the FGDS model and RGDS model under various working conditions. The frequencies of radial accelerations of support bearings are analyzed here. Figure 6 shows the comparisons of accelerations of RGDS model and FGDS model. The input shaft rotate speed is 2000r/min; and the output torque is 500N·m. In Figure 6, under the same working conditions, the acceleration amplitude of RGDS model is higher than that of FGDS model. The reason for this phenomenon is that the rotor structural damping is ignored in the RGDS model.

Moreover, the bending and shear deformations of the rotor during the operation are ignored. The external force will only change the rotor translation acceleration. This will cause the acceleration obtained by the RGDS model is higher than the one obtained by the FGDS model. Figure 7 shows the comparisons of spectra of Y -direction accelerations of each bearing's outer ring from the FGDS model and RGDS model when the input shaft rotate speed is 2000r/min. In Figure 7, the spectra of accelerations of bearings on the input shaft are the meshing frequency f_{m1} ($f_{m1}=f_{s1}\times Z_1=33.33\times 39=1300\text{Hz}$) of gear#1 and gear#2; and its harmonics are $2f_{m1}$. The spectra of accelerations of bearings on the intermediate shaft include the meshing frequency f_{m1} , meshing frequency f_{m2} ($f_{m2}=f_{s2}\times Z_3=11.11\times 44=488.8\text{Hz}$) of gear#3 and gear#4, and the harmonics $2f_{m1}$ and $2f_{m2}$. The spectra of accelerations of bearings on the output shaft also contain f_{m1} , f_{m2} and their harmonics, as well as the rotation frequency of input shaft f_{s1} . The peak amplitudes of spectra of accelerations of each bearing from the RGDS model are higher than those from the FGDS model. The roller passing frequency of the outer raceway harmonics $3f_{o1}$ and the roller passing frequency of the inner raceway harmonics $3f_{i1}$ can be also found in bearing #1 and bearing #2. The reason of this phenomenon is that the bearing is considered to have waviness error, whose waviness number is 18. The velocities of second and third shaft are relatively low. Thus, the roller passing frequency of the outer raceway and inner raceway are not obvious.

Figure 8 shows the comparisons of spectra of Y -direction acceleration of each bearing's outer ring from the FGDS model and RGDS model when the input shaft rotate speed is 2500r/min. In Figure 6, the spectra of accelerations of bearings on the input shaft are the meshing frequency f_{m1} ($f_{m1}=f_{s1}\times Z_1=41.66\times 39=1625\text{Hz}$) of gear#1 and gear#2; and its harmonics are $2f_{m1}$. The spectra of accelerations of bearings on the intermediate shaft includes the meshing frequency f_{m1} , meshing frequency f_{m2} ($f_{m2}=f_{s2}\times Z_3=13.88\times 44=611.1\text{Hz}$) of gear#3 and gear#4, and the harmonics $2f_{m1}$ and $2f_{m2}$. The spectra of accelerations of bearings on the output shaft also contain f_{m1} , f_{m2} and their harmonics, as well as the rotation frequency of input shaft f_{s1} . The peak amplitudes of spectra of accelerations of each bearing from the RGDS model are higher than those from the FGDS model, especially for the bearing#1 and bearing#6. The roller passing frequency of the outer raceway harmonics $3f_{o1}$ and the roller passing frequency of the inner raceway harmonics $3f_{i1}$ can be also found in bearing #1 and bearing #2. The reason of this phenomenon is that the bearing is considered to have waviness error, whose waviness number is 18. The velocities of second and third shaft are relatively low. Thus, the roller passing frequency of the outer raceway and inner raceway are not obvious.

Figure 9 shows the comparisons of spectra of Y -direction acceleration of each bearing's outer ring from the FGDS model and RGDS model when the input shaft rotate speed is 3000r/min. In Figure 7, the spectra of accelerations of bearings on the input shaft are the meshing frequency f_{m1} ($f_{m1}=f_{s1}\times Z_1=50\times 39=1950\text{Hz}$) of gear#1 and gear#2; and its harmonics are $2f_{m1}$. The spectra of accelerations of bearings on the intermediate shaft include the meshing frequency f_{m1} , meshing frequency f_{m2} ($f_{m2}=f_{s2}\times Z_3=16.66\times 44=733.3\text{Hz}$) of gear#3 and gear#4, and the harmonics $2f_{m1}$ and $2f_{m2}$. The spectra of accelerations of bearings on the output shaft also contain f_{m1} , f_{m2} and their harmonics, as well as the rotation frequency of input shaft f_{s1} . The peak amplitudes of spectra of accelerations of each bearing from the RGDS model are higher than those from the FGDS model, especially for the bearing#1 and bearing#6. The roller passing frequency of the outer raceway harmonics $3f_{o1}$ and the roller passing frequency of the inner raceway harmonics $3f_{i1}$ can be also found in bearing #1 and bearing #2. The reason of this phenomenon is that the bearing is considered to have waviness error, whose waviness number is 18. The velocities of second and third shaft are relatively low. Thus,

the roller passing frequency of the outer raceway and inner raceway are not obvious.

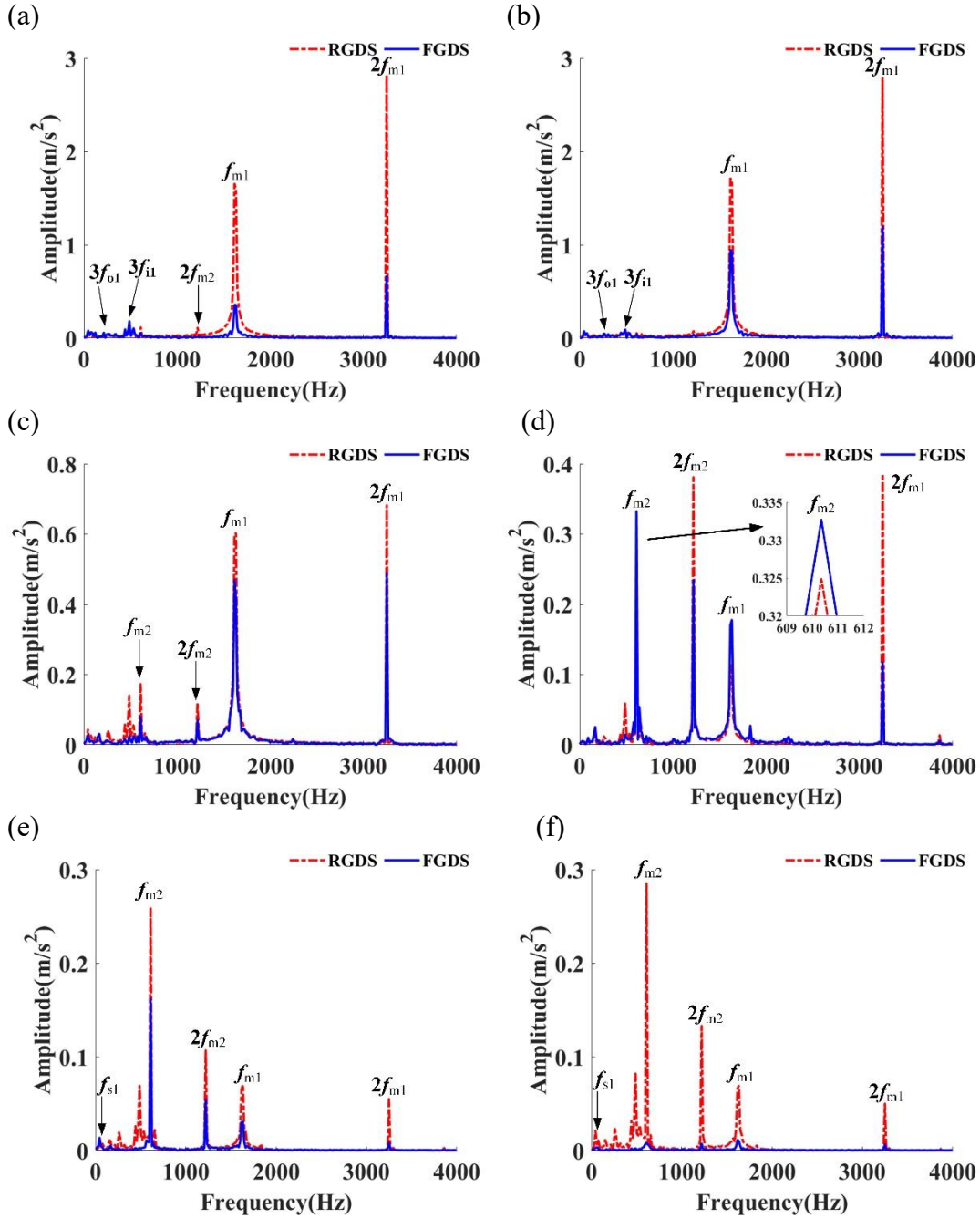


Fig 8. Comparisons of frequency-domain accelerations of support bearings from the FGDS model and RGDS model in the Y direction when the input shaft rotate speed is 2500r/min. (a) Bearing#1, (b) bearing#2, (c) bearing#3, (d) bearing#4, (e) bearing#5, and (f) bearing#6.

Figure 10 shows the comparisons of spectra of Y -direction acceleration of each bearing's outer ring from the FGDS model and RGDS model when the input shaft rotate speed is 3500r/min. In Figure 8, the spectra of acceleration of bearings on the input shaft are the meshing frequency f_{m1} ($f_{m1}=f_{s1}\times Z_1=58.33\times 39=2275\text{Hz}$) of gear#1 and gear#2; and its harmonics are $2f_{m1}$. The spectra of accelerations of bearings on the intermediate shaft include the meshing frequency f_{m1} , meshing frequency f_{m2} ($f_{m2}=f_{s2}\times Z_3=19.44\times 44=855.6\text{Hz}$) of gear#3 and gear#4, and the harmonics $2f_{m1}$ and $2f_{m2}$. The spectra of accelerations of bearings on the output shaft also contain f_{m1} , f_{m2} and their harmonics, as well as the rotation frequency of input shaft f_{s1} . The peak amplitudes

of spectra of accelerations of each bearing from the RGDS model are higher than those from the FGDS model, especially for the bearing#1 and bearing#6. The roller passing frequency of the outer raceway harmonics $3f_{o1}$ and the roller passing frequency of the inner raceway harmonics $3f_{i1}$ can be also found in bearing #1 and bearing #2. The reason of this phenomenon is that the bearing is considered to have waviness error, whose waviness number is 18. The velocities of second and third shaft are relatively low. Thus, the roller passing frequency of the outer raceway and inner raceway are not obvious.

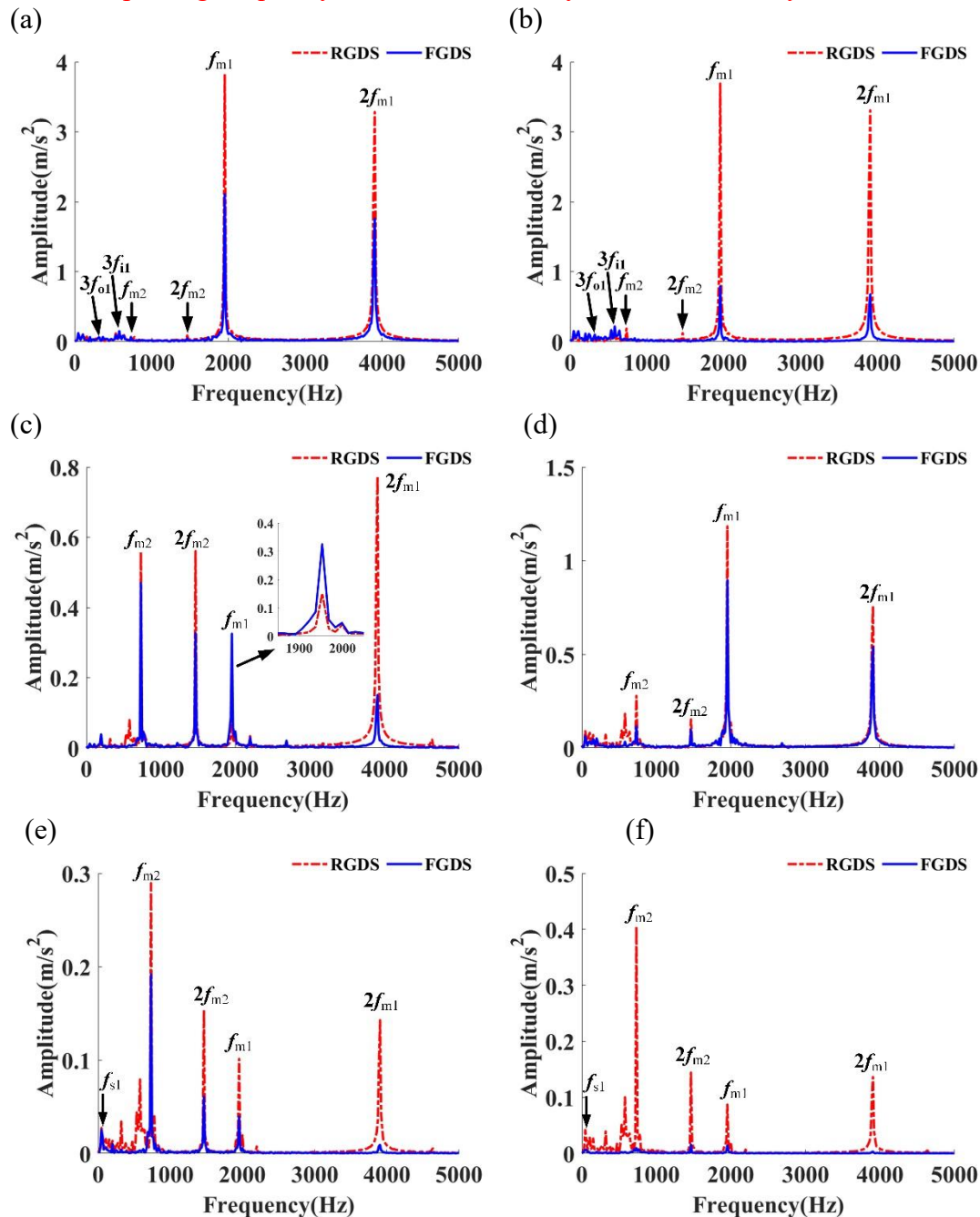


Fig 9. Comparisons of frequency-domain accelerations of support bearings from the FGDS model and RGDS model in the Y direction when the input shaft rotate speed is 3000r/min. (a) Bearing#1, (b) bearing#2, (c) bearing#3, (d) bearing#4, (e) bearing#5, and (f) bearing#6.

Figure 11 shows the comparisons of spectra of Y-direction accelerations of each bearing's outer ring from the FGDS model and RGDS model when the input shaft rotate speed is 4000r/min. In Figure 9, the spectra of accelerations of bearings on the input

shaft are the meshing frequency f_{m1} ($f_{m1}=f_{s1}\times Z_1=66.66\times 39=2599.7\text{Hz}$) of gear#1 and gear#2; and its harmonics are $2f_{m1}$. The spectra of accelerations of bearings on the intermediate shaft include the meshing frequency f_{m1} , meshing frequency f_{m2} ($f_{m2}=f_{s2}\times Z_3=22.22\times 44=977.8\text{Hz}$) of gear#3 and gear#4, and the harmonics $2f_{m1}$ and $2f_{m2}$. The spectra of accelerations of bearings on the output shaft also contain f_{m1} , f_{m2} and their harmonics, as well as the rotation frequency of input shaft f_{s1} . The peak amplitudes of spectra of accelerations of each bearing from the RGDS model are higher than those from the FGDS model, especially for the bearing#1 and bearing#6. **The roller passing frequency of the outer raceway harmonics $3f_{o1}$ and the roller passing frequency of the inner raceway harmonics $3f_{i1}$ can be also found in bearing #1 and bearing #2.** The reason of this phenomenon is that the bearing is considered to have waviness error, whose waviness number is 18. The velocities of second and third shaft are relatively low. Thus, the roller passing frequency of the outer raceway and inner raceway are not obvious.

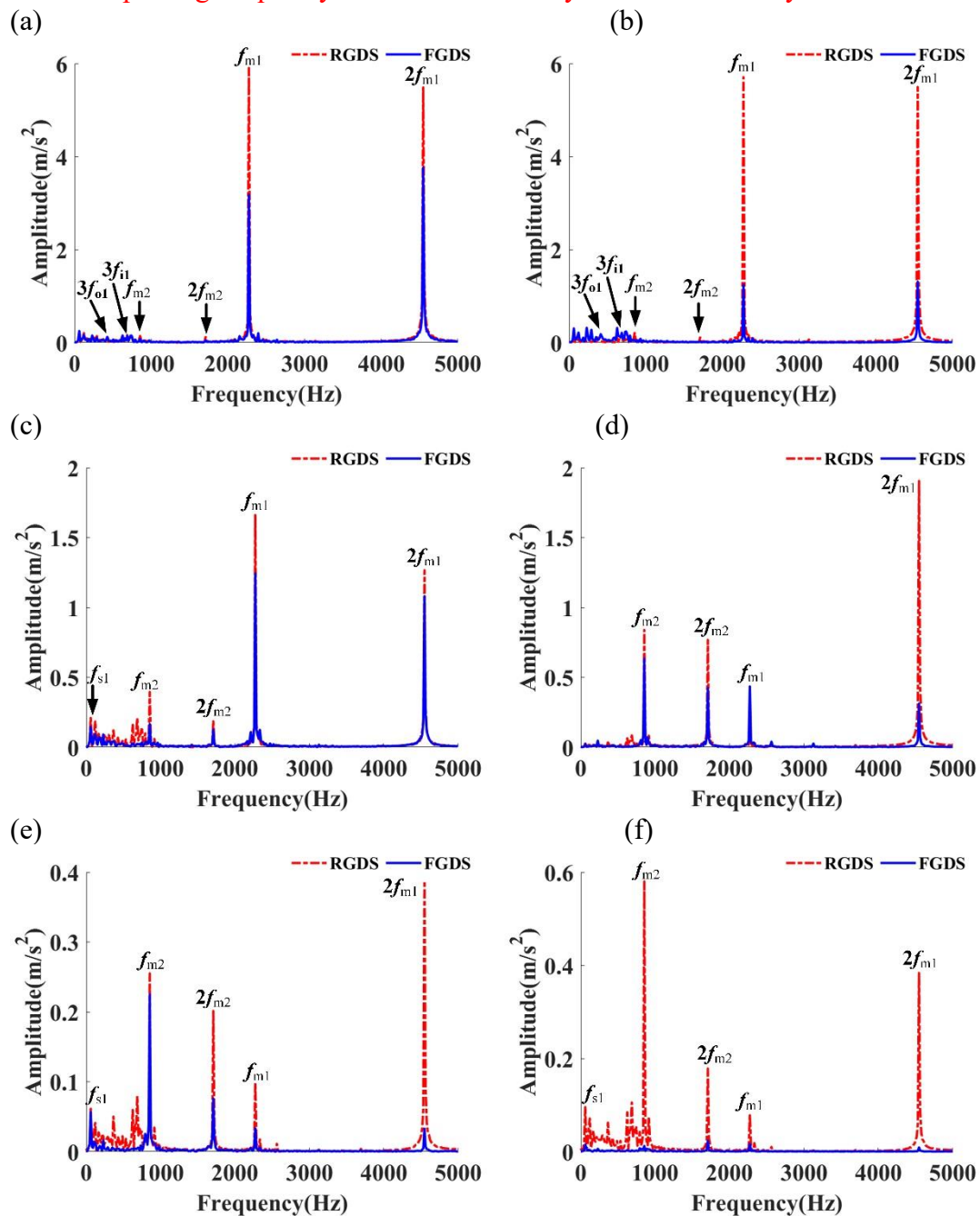


Fig 10. Comparisons of frequency-domain accelerations of support bearings from the

FGDS model and RGDS model in the Y direction when the input shaft rotate speed is 3500r/min. (a) Bearing#1, (b) bearing#2, (c) bearing#3, (d) bearing#4, (e) bearing#5, and (f) bearing#6.

Figure 12 shows the comparisons of RMS values of Y -direction accelerations of each bearing's outer ring from the FGDS model and RGDS model when the input shaft rotate speed is form 2000r/min to 4000r/min; and the output torque is 500N·m. The calculation method for the RMS value is given in Ref. [39]. In Figure 10, the RMS values of RGDS model are much higher than those of FGDS model especially for bearing#6's RMS; and both the RMS values of RGDS model and FGDS model increase with the increment of input rotate speed.

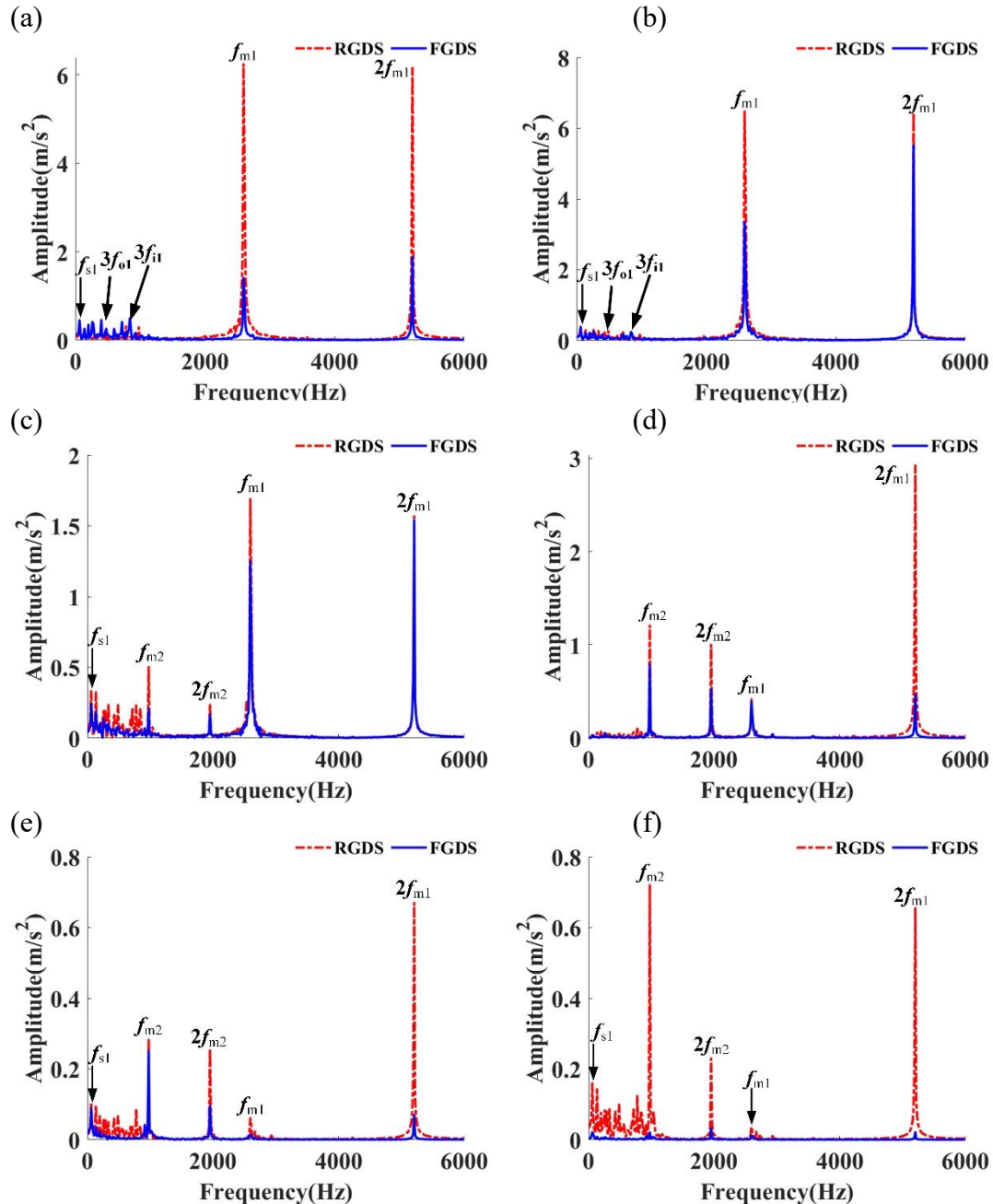


Fig 11. Comparisons of frequency-domain accelerations of support bearings from the FGDS model and RGDS model in the Y direction when the input shaft rotate speed is 4000r/min. (a) Bearing#1, (b) bearing#2, (c) bearing#3, (d) bearing#4, (e) bearing#5, and (f) bearing#6.

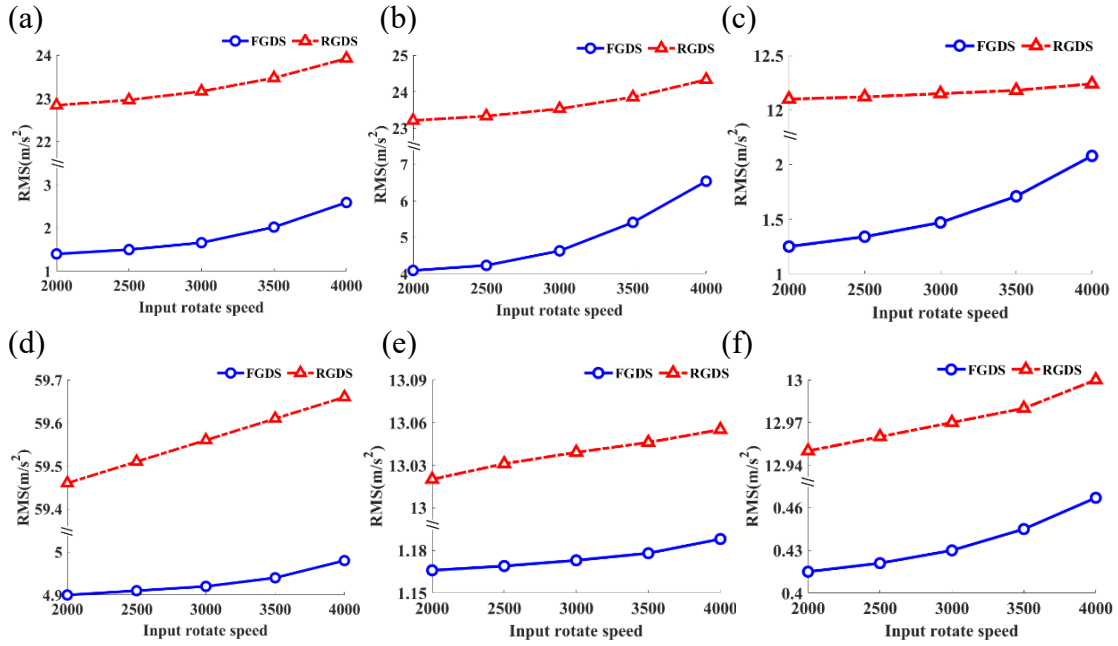


Fig 12. Comparisons of RMS values of support bearings from the FGDS model and RGDS model in the Y direction. (a) Bearing#1, (b) bearing#2, (c) bearing#3, (d) bearing#4, (e) bearing#5, and (f) bearing#6.

3.2 Vibrations analysis of FGDS in Z direction

In this section, the vibrations of FGDS in Z direction obtained by the proposed model and the RGDS model are compared. Figure 13 gives the accelerations obtained by the RGDS model and FGDS model when the input shaft rotate speed is 2000r/min. The acceleration amplitude in Z direction of FGDS model is higher than that of RGDS model. Moreover, the accelerations in Z direction are less than the ones in Y direction. The reason for this phenomenon is that the meshing force radial component is larger than the axial component. Figure 14 gives the comparisons of spectra of Z direction accelerations of each bearing's outer ring from the FGDS model and RGDS model when the input shaft rotate speed is 2000r/min. In Fig. 14, the spectra of accelerations of bearings are the meshing frequency f_{m1} ($f_{m1}=f_{s1}\times Z_1=33.33\times 39=1300\text{Hz}$) of gear #1 and meshing frequency f_{m2} ($f_{m2}=f_{s2}\times Z_3=11.11\times 44=488.8\text{Hz}$) of gear #2, their harmonics $2f_{m1}$ and $2f_{m2}$, and $f_{m1}\pm f_{m2}$. The amplitudes of these frequencies obtained by the FGDS model are larger than that of the RGDS model. These are opposite to the results in Y direction. The reason for this phenomenon is that the stiffness in Z direction is higher than Y direction. Thus, the vibrations in Z direction are more sensitive to the change of external force. The meshing deformation in the FGDS model is higher than the one in the RGDS model. The RGDS model can be considered to have large stiffness. The axial stiffness of RGDS model is higher than the one of FGDS model. However, the meshing forces in the FGDS model are larger than the ones of RGDS model. The increases of meshing forces have a more significant effect on the vibrations in Z direction. The radial stiffness of RGDS model is much higher than the one of FGDS model. Thus, the acceleration amplitude in Z direction of FGDS model is higher than that of RGDS model, but the acceleration amplitude in Y direction of FGDS model is less than that of RGDS model.

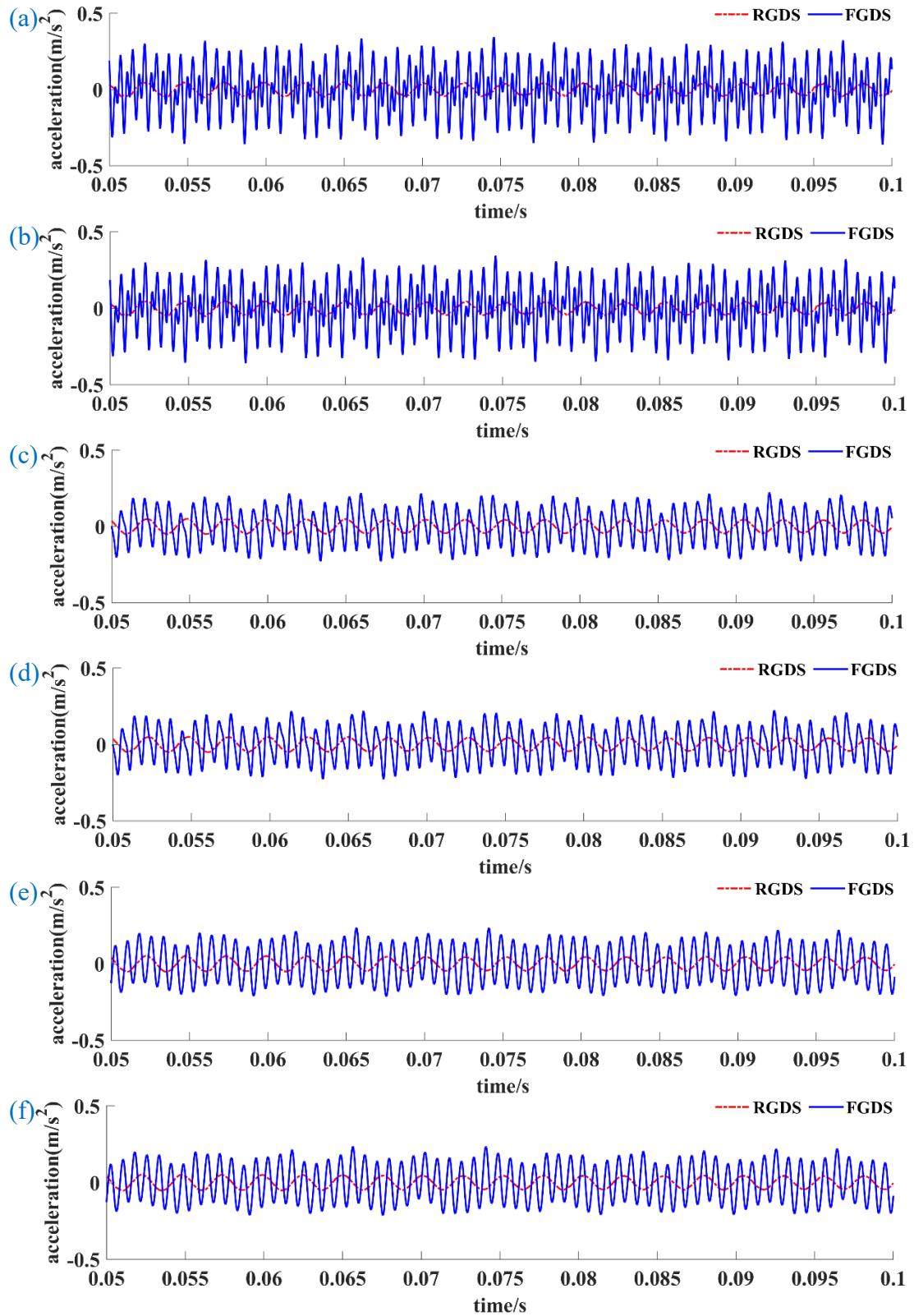


Fig 13. Comparisons of time-domain accelerations of support bearings from FGDS model and RGDS model in the Z direction. (a) Bearing#1, (b) bearing#2, (c) bearing#3, (d) bearing#4, (e) bearing#5, and (f) bearing#6.

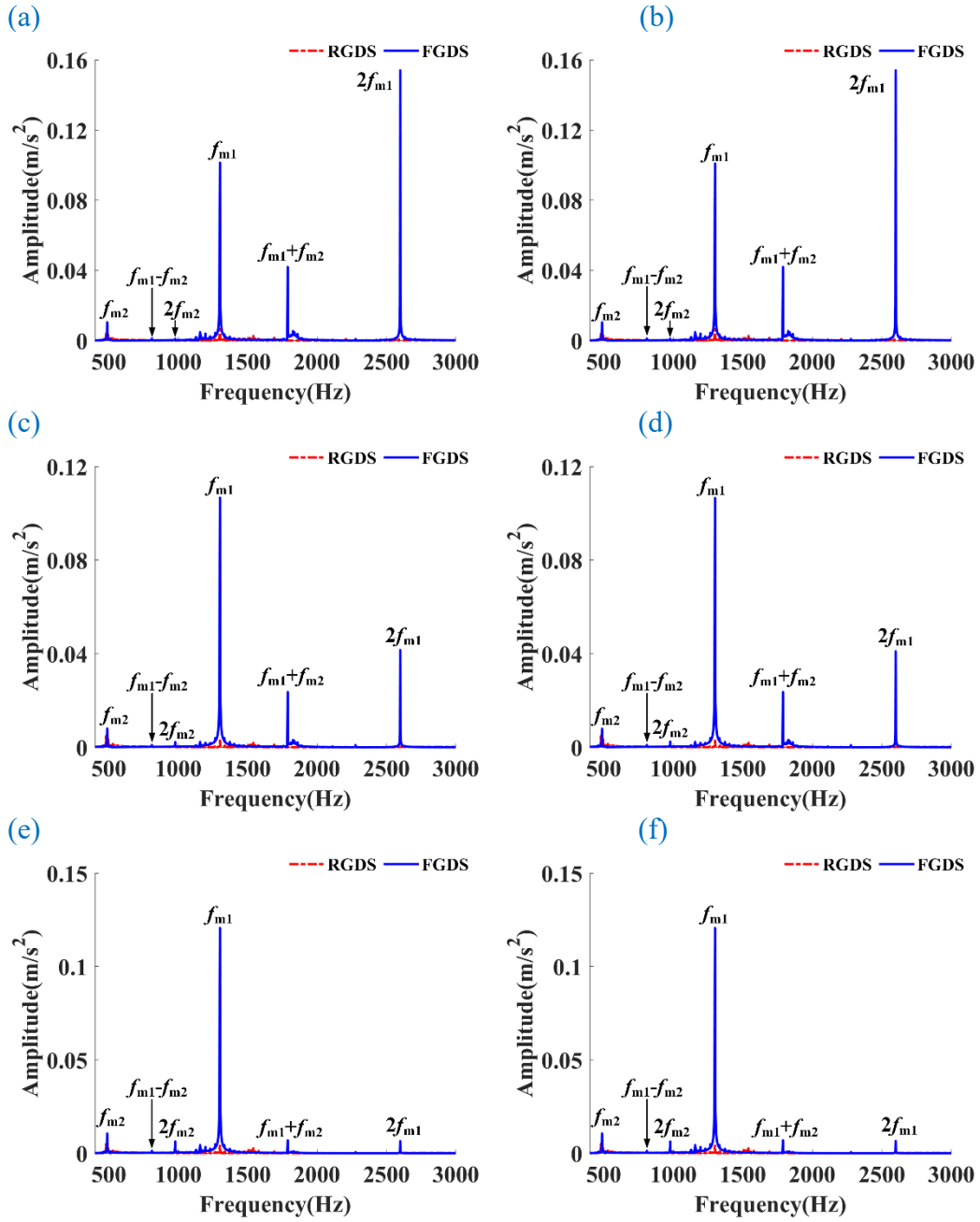


Fig 14. Comparisons of frequency-domain accelerations of support bearings from the FGDS model and RGDS model in the Y direction. (a) Bearing#1, (b) bearing#2, (c) bearing#3, (d) bearing#4, (e) bearing#5, and (f) bearing#6.

Figure 14 shows the comparisons of RMS values of Z-direction accelerations of each bearing's outer ring from the FGDS model and RGDS model when the input shaft rotate speed is form 2000r/min to 4000r/min; and the output torque is 500N·m. In Fig. 15, the RMS values of FGDS model are much higher than those of RGDS model; and both the RMS values of RGDS model and FGDS model increase with the increment of input rotate speed.

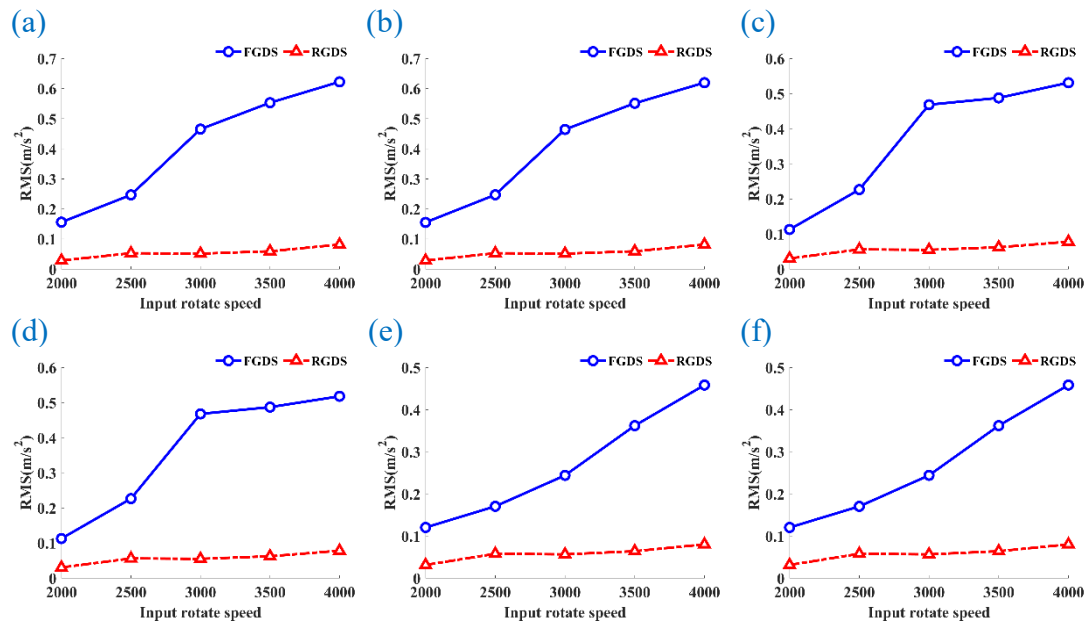
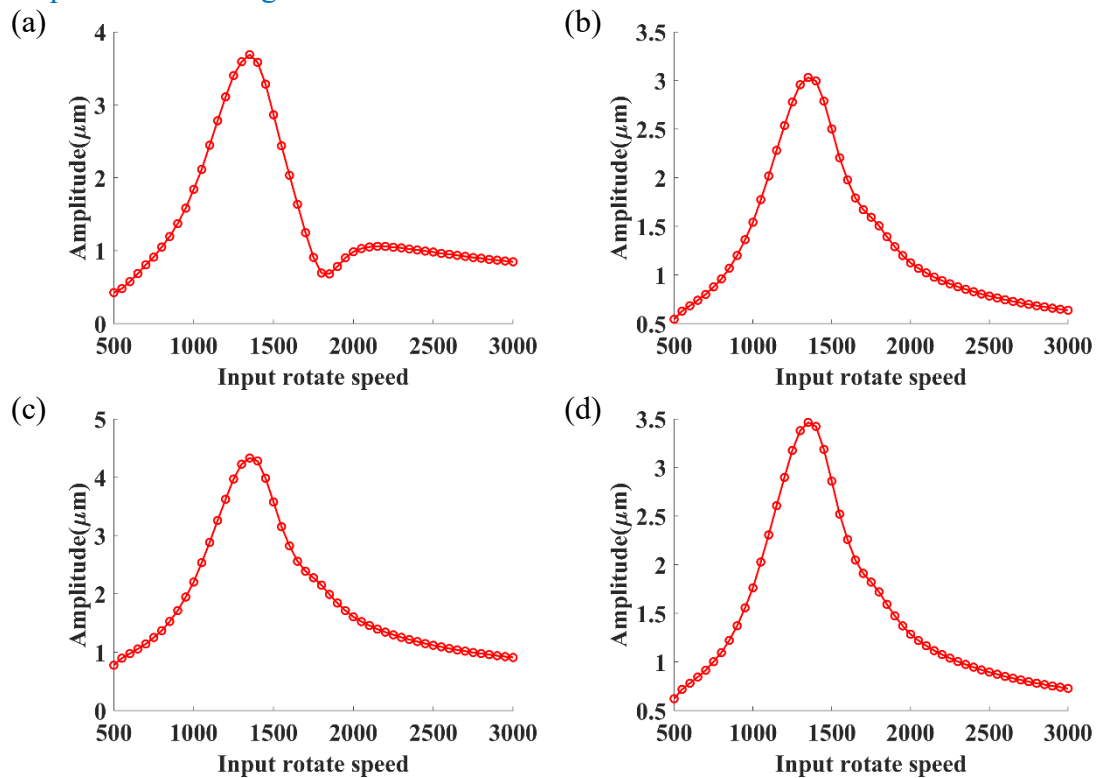


Fig 15. Comparisons of RMS values of support bearings from the FGDS model and RGDS model in the Z direction. (a) Bearing#1, (b) bearing#2, (c) bearing#3, (d) bearing#4, (e) bearing#5, and (f) bearing#6.

3.3 Frequency-amplitude characteristics analysis

In Fig. 16, the frequency-amplitude characteristics of bearing #1, bearing #2, bearing #3, bearing #4, bearing #5, and bearing #6 are given. The resonance peak appears in 1350r/min. The peak amplitudes of bearing #1, bearing #2, bearing #3, bearing #4, bearing #5 and bearing #6 are 3.69 μm , 3.03 μm , 4.33 μm , 3.46 μm , 3.82 μm and 3.44 μm , respectively. The peak amplitude of bearing #3 is the maximum. The peak amplitude of bearing #2 is the minimum.



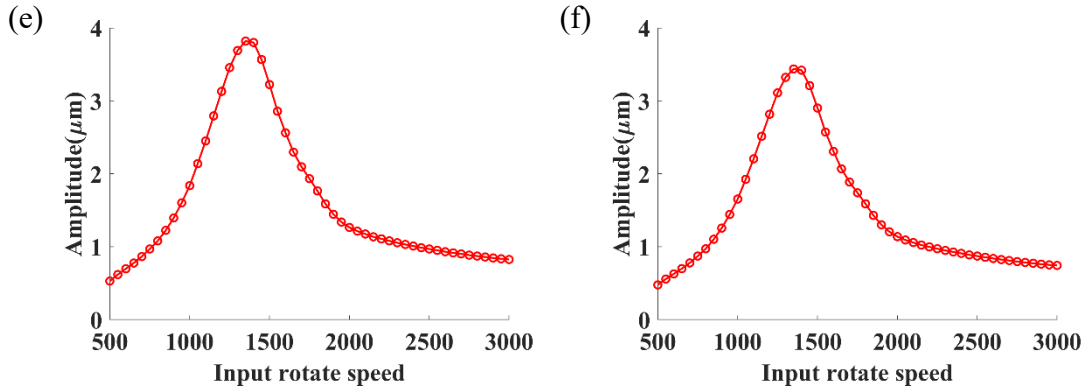


Fig. 16. Frequency-amplitude characteristics of (a) bearing#1, (b) bearing#2, (c) bearing#3, (d) bearing#4, (e) bearing#5, and (f) bearing#6.

4 Conclusions

In this paper, a FGDS model of the multi-stage transmission system is established. The shafts' transverse, longitudinal and torsional vibrations are all considered. The Timoshenko beam element with 6 DOFs is used to establish the dynamic model of shaft segment element. The lumped parameter method is used to establish gear and bearing dynamic models. The vibrations of the multi-stage transmission system in Y (radial direction) and Z (axial direction) directions are analyzed. An experiment is conducted to prove the correctness of the proposed model. The analysis results may give a new method to decrease the vibrations and improve the quality of GTSs. The conclusions are as follows.

1) The characteristic frequency errors of measured acceleration spectrum and simulated acceleration spectrum are less than 1%. The simulation results and experimental results are in good agreement, and this indicates the correctness of the proposed model to a certain extent.

2) Due to the RGDS model ignores the shaft structural damping and considers the structural stiffness is very large, the acceleration amplitude of RGDS model in Y direction is higher than that of FGDS model.

3) Due to the meshing forces in the FGDS model are larger than the ones of RGDS model, the acceleration amplitude of RGDS model in Z direction is less than that of FGDS model. This is opposite to the results in Y direction because that the increases of meshing forces have a more significant effect on the vibrations in Z direction, but the radial stiffnesses have a more significant effect on the vibrations in Y direction.

4) In the spectra in Y direction, the meshing frequencies (f_{m1} and f_{m2}) and their harmonics ($2f_{m1}$ and $2f_{m2}$) can be found. In the spectra in Z direction, f_{m1} , f_{m2} , $2f_{m1}$, $2f_{m2}$, and $f_{m1} \pm f_{m2}$ can be found.

5) When the input shaft rotates speed increases, the vibrations of FGDS model and RGDS model have the tendency of increasing. Compared with the RGDS model, the amplitude and waveform of different positions of FGDS model have more differences. Therefore, the dynamic model of GTS considering the shaft flexibility can show the vibration differences of GTS at different positions, which is more authentic and reliable.

Funding

Support provided by the National Natural Science Foundation of China under Contract No. 52175120 and 52211530085; Natural Science Foundation of Chongqing Contract No. CSTB2022NSCQ-MSX0318; and the Fundamental Research Funds for the Central Universities.

Conflict of Interest

The author declared that he has no conflicts of interest.

References

- [1] Dong P, Zuo S, Tenberge P, et al. Rapid hob tip corner optimization of spur gears for increasing bending strength. *International Journal of Mechanical Sciences*, 2022, 224: 107322.
- [2] Wu W, Wei C H, Yuan S H. Numerical simulation of ball bearing flow field using the moving particle semi-implicit method, *Engineering Applications of Computational Fluid Mechanics*, 2022, 16(1): 215-228.
- [3] Liu J, Xu Z D. A simulation investigation of lubricating characteristics for a cylindrical roller bearing of a high-power gearbox. *Tribology International*, 2022, 167: 107373.
- [4] Neriya S. V, Bhat R. B, Sankar T. S. The coupled torsional-flexural vibration of a geared shaft system using finite element method. *The Shock and Vibration Bulletin*, 1985, 55(3): 13-25.
- [5] Zhu C, Xu X, and Liu H. Research on dynamical characteristics of wind turbine gearboxes with flexible pins. *Renewable Energy*, 2014, 68(8): 724-732.
- [6] Liu J, Liu S, Zhao W, Zhang L. Dynamic characteristics of spur gear pair with dynamic center distance and backlash. *International Journal of Rotating Machinery* 2019, 2019: 1-9.
- [7] Ian Howard, S X Jia. The dynamic modeling of a spur gear in mesh including friction and a crack. *Mechanical Systems and Signal Processing*, 2001, 15(5): 831-853.
- [8] Mohammed OD, Rantatalo M. Dynamic modelling of a one-stage spur gear system and vibration-based tooth crack detection analysis. *Mechanical Systems and Signal Processing*, 2015, 54: 293–305.
- [9] Bozca M. Transmission error model-based optimisation of the geometric design parameters of an automotive transmission gearbox to reduce gear rattle noise. *Applied Acoustics*, 2018, 130: 247–59.
- [10] Theodossiades S, De la Cruz M, and Rahnejat H. Prediction of airborne radiated noise from lightly loaded lubricated meshing gear teeth. *Applied Acoustics*, 2015, 100: 79–86.
- [11] Dikmen E, van der Hoogt P, de Boer A, et al. A flexible rotor on flexible supports: modeling and experiments. *ASME 2009 International Mechanical Engineering Congress and Exposition. American Society of Mechanical Engineers Digital Collection*, 2010: 51-56.
- [12] Xi S, Cao H, Chen X, et al. A dynamic modeling approach for spindle bearing system supported by both angular contact ball bearing and floating displacement bearing. *Journal of Manufacturing Science and Engineering*, 2018, 140(2): 021014.
- [13] Xi S, Cao H, Chen X. Dynamic modeling of spindle bearing system and vibration response investigation. *Mechanical Systems and Signal Processing*, 2019, 114: 486-511.
- [14] Hamzehlouia Sina. Squeeze film dampers supporting high-speed rotors: Rotor dynamics. *Journal of Engineering Tribology*, 2021, 235(3): 495-508.
- [15] Nan G, Zhang Y, Zhu Y, et al. Nonlinear dynamics of rotor system supported by bearing with waviness. *Science Progress*, 2020, 103(3): 0036850420944092.
- [16] Y. Liu, Z. Chen, L. Tang, et al. Skidding dynamic performance of rolling bearing with cage flexibility under accelerating conditions. *Mechanical Systems and Signal Processing*, 2021, 150: 107257.
- [17] Liu J, R. Pang, S. Ding, et al. Vibration analysis of a planetary gear with the flexible ring and planet bearing fault. *Measurement*, 2020, 165: 108100.
- [18] Liu J, Shao Y. Dynamic modeling for rigid rotor bearing systems with a localized defect considering additional deformations at the sharp edges. *Journal of Sound and*

- Vibration, 2017, 398: 84–102.
- [19] Sinou J, Villa C, Thouverez F, et al. Experimental analysis of the dynamical response of a flexible rotor including the effects of external damping. *Journal of Engineering and Applied Sciences*, 2006, 1(4): 483-490.
- [20] Cao H, Li Y, Chen X. A new dynamic model of ball-bearing rotor systems based on rigid body element. *Journal of Manufacturing Science and Engineering*, 2016, 138(7): 071007.
- [21] Liu J. A stiffness optimization method for a shaft-bearing-pedestal system based on the dynamics. *Journal of Multi-body Dynamics*, 2021, 235(2): 235-245.
- [22] Liu J, Wang L F, Shi Z F. Dynamic modelling of the defect extension and appearance in a cylindrical roller bearing. *Mechanical Systems and Signal Processing*, 2022, 173(3):109040.
- [23] Li Y, Luo Z, Liu J, et al. Dynamic modeling and stability analysis of a rotor-bearing system with bolted-disk joint. *Mechanical Systems and Signal Processing*, 2021, 158: 107778.
- [24] Jin Y, Lu K, Huang C, et al. Nonlinear dynamic analysis of a complex dual rotor-bearing system based on a novel model reduction method. *Applied Mathematical Modelling*, 2019, 75: 553-571.
- [25] Liu J, Tang C, Pan G. Dynamic modeling and simulation of a flexible-rotor ball bearing system. *Journal of Vibration and Control*, 2022, 28(23-24): 3495-3509.
- [26] Cao H, Shi F, Li Y, et al. Vibration and stability analysis of rotor-bearing-pedestal system due to clearance fit. *Mechanical Systems and Signal Processing*, 2019, 133: 106275.
- [27] Wang S, Zhu R. Study on load sharing behavior of coupling gear-rotor-bearing system of GTF aero-engine based on multi-support of rotors. *Mechanism and Machine Theory*, 2020, 147: 103764.
- [28] Kong X, Hu Z, Tang J, et al. Effects of gear flexibility on the dynamic characteristics of spur and helical gear system. *Mechanical Systems and Signal Processing*, 2023, 184: 109691.
- [29] Hu Z, Tang J, Wang Q, et al. Investigation of nonlinear dynamics and load sharing characteristics of a two-path split torque transmission system. *Mechanism and Machine Theory*, 2020, 152: 103955.
- [30] Huangfu Y, Zeng J, Ma H, et al. A flexible-helical-gear rotor dynamic model based on hybrid beam-shell elements. *Journal of Sound and Vibration*, 2021, 511: 116361.
- [31] Wan Z, Cao H, Zi Y, et al. Mesh stiffness calculation using an accumulated integral potential energy method and dynamic analysis of helical gears. *Mechanism and Machine Theory*, 2015, 92: 447-463.
- [32] Babu C K, Tandon N, Pandey R K. Nonlinear vibration analysis of an elastic rotor supported on angular contact ball bearings considering six degrees of freedom and waviness on balls and races. *Journal of Vibration and Acoustics*, 2014, 136(4): 044503-1-5.
- [33] Vazquez J A, Barrett L E, Flack R D. A flexible rotor on flexible bearing supports: stability and unbalance response. *Journal of Vibration and Acoustics*, 2001, 123(4):137-144.
- [34] Jiang H, Liu F. Mesh stiffness modelling and dynamic simulation of helical gears with tooth crack propagation. *Meccanica*, 2020, 55(6): 1215-1236.
- [35] Wang H, Han Q, Zhou D. Output torque modeling of control moment gyros considering rolling element bearing induced disturbances. *Mechanical Systems and Signal Processing*, 2019, 115: 188-212.

- [36] Liu J, Xu Y, Pan G. A combined acoustic and dynamic model of a defective ball bearing. *Journal of Sound and Vibration*, 2021, 501: 116029.
- [37] Liu J, Tang C, Wu H, et al. An analytical calculation method of the load distribution and stiffness of an angular contact ball bearing. *Mechanism and Machine Theory*, 2019, 142: 103597.
- [38] Liu J, Ni H, Zhou R, Li X, Xing Q, and Pan G. A simulation analysis of ball bearing lubrication characteristics considering the cage clearance. *Journal of Tribology*, 2023, 145(4): 044301.
- [39] Liu J, Xu Z, Zhou L, et al. A statistical feature investigation of the spalling propagation assessment for a ball bearing. *Mechanism and Machine Theory*, 2019, 131: 336-350.